Tidal energy resource characterization: methodology and field study in Admiralty Inlet, Puget Sound, US

Polagye, B.[1] and Thomson, J.[2]

[1]Northwest National Marine Renewable Energy Center, Department of Mechanical Engineering

[2] Northwest National Marine Renewable Energy Center, Applied Physics Laboratory

University of Washington, Seattle, WA 98115

Abstract

Tidal energy resource characteristics are presented from a multi-year field study in northern Admiralty Inlet, Puget Sound, WA (USA). Measurements were conducted as part of a broader effort to characterize the physical and biological environment at this location ahead of a proposed tidal energy project. The resource is conceptually partitioned into deterministic, meteorological, and turbulent components. Metrics with implications for device performance are used to describe spatial variations in the tidal resource. The performance differences between passive and fixed yaw turbines are evaluated at these locations. Results show operationally significant variations in the tidal resource over length scales less than 100 m, likely driven by large eddies shed from a nearby headland. Finite-record length observations of tidal currents are shown to be acceptable for estimating device performance, but unsuitable for direct investigation of design loads.

Keywords: tidal energy; hydrokinetic; resource characterization

1 Introduction

The need for sustainable energy sources has driven an interest in all types of renewable energy, including tidal hydrokinetic energy, whereby the kinetic energy of strong (> 1 m/s) tidal currents is converted to electricity. The devices used to achieve this are superficially similar to wind turbines and share common physical and mechanical principles. The global tidal energy resource is relatively modest at 3.7 TW and the practically extractable resource will be several orders of magnitude lower [**1**]. Typically, economically attractive tidal energy sites are located at relative geographic constrictions (narrows or sills) and the resource is localized over length scales on the order of kilometers. In comparison, economically viable wind and wave resources are distributed over hundreds of kilometers. These limitations are offset by the first-order predictability of the tidal resource, high average resource intensity (> 1 kW m^{-2}), and the ability to leverage over forty years of experience from wind energy and offshore oil and gas exploration.

Resource characterization is an early-stage project development activity. One objective is to evaluate the power generation potential for a turbine at a particular location. Another is to establish design loads. A number of tidal first-generation turbine failures are ascribed to improper characterization of design loads.

Acoustic Doppler current profilers (ADCPs) are a standard instrument used to measure three-dimensional currents throughout the water column. ADCPs measure currents indirectly through the time dilation of backscattered acoustic pulses [**2**]. Pulses along 3 or 4 divergent beams return

the velocity projection along each beam. The velocity projections are then used to reconstruct the full three-dimensional velocity field, and a coordinate transformation based on instrument orientation (heading, pitch, and roll) converts these measurements to a geographic reference frame,

$$U = u\hat{i} + v\hat{j} + w\hat{k}, \tag{1.1}$$

where *u*, *v*, and *w* are the north, east, and upward components of measured velocity. Because of the finite pulse length, each of these velocities includes a degree of measurement uncertainty or "Doppler noise" [**3**]. Averaging the results from multiple pulses reduces this uncertainty, providing a more accurate estimate of the mean velocity over a sampling interval. Doppler noise has a zero mean value and known standard deviation, n_{sample}. Doppler velocimeters and electromagnetic current meters, both of which measure velocity at a point, have also been used to lesser extent in resource characterization studies.

Measured currents ($\boldsymbol{U_{sample}}$) are conceptually partitioned into deterministic ($\boldsymbol{U_{det}}$), meteorological ($\boldsymbol{U_{met}}$), and turbulent ($\boldsymbol{U_{turb}}$) components,

$$U_{\mathbf{sample}} = U_{\text{det}} + U_{\mathbf{met}} + U_{\mathbf{turb}} \pm n_{\mathbf{sample}}. \tag{1.2}$$

each of which are further subdivided. The deterministic currents include harmonic currents, described by harmonic constituents [**4**,**5**], as well as the aharmonic response to these currents induced by local topography and bathymetry. Aharmonic currents are not described by tidal constituents, but are repeatable, site-specific flow features [**6**]. Meteorological currents include wave- and wind-induced motion [**7**,**8**], residual currents associated with estuarine stratification [**9**], and storm surges [**10**]. Turbulent currents include large-scale, horizontal eddies and small-scale, isotropic turbulence [**11**]. The relative contribution of these elements to measured currents is site-specific.

This paper presents results from a multi-year tidal energy resource characterization field study in northern Admiralty Inlet, Puget Sound, WA (USA) at the site of a proposed tidal energy project. Characterization metrics are used to quantify variations in the tidal resource over a range of spatial and temporal scales. Variations in the deterministic and meteorological currents are emphasized; turbulence characteristics are described elsewhere [**11**]. The number and duration of stationary ADCP deployments at this location is more intensive than typical for site development. Consequently, these data provide insight into the variability that may be undersampled by common tidal energy siting practices. In combination with a simple turbine model, the operational significance of resource variability is evaluated and the performance of passive and fixed yaw turbines compared. This paper extends the resource metrics described in [**12**] by quantifying the error associated with their calculation from finite-length records.

2 Methodology

2.1 Field Measurements

Admiralty Inlet is a major sill at the mouth of Puget Sound. Excepting the relatively small exchange through Deception Pass, the entirety of the Puget Sound tidal prism passes through this constriction. Between Point Wilson and Admiralty Head, the channel cross-section is at a minimum and current amplitude at a maximum. ADCPs were deployed repeatedly in an upward looking configuration on ballasted fiberglass tripods (Oceanscience Sea Spiders) for periods of up to three months each. The instrument head is approximately 0.7 m above the seabed and the blanking distances varied between 0.4 and 1.0 m, depending on the operating frequency of the profiler. Sea Spiders were lowered to the seabed and as-deployed locations recorded by DGPS. Wire angles were minimized by drifting during deployments and recovery positions were typically within 5 m of as-deployed locations (i.e., within DGPS error). Details of each deployment are given in Table 1 and locations shown in Figure 1. Site 1 is a composite record consisting of four deployments, each approximately 3 months in duration and located within a 20 m radius. Doppler noise in each sample (n_{sample}) is calculated by the manufacturer's software.

Velocity measurements were a component of studies to broadly characterize the physical and biological environment at this location prior to tidal turbine installation. Locations were selected based on shipboard ADCP surveys, power cable routing considerations for the proposed project, vessel traffic patterns, and biological characterization studies. Spatial variability in the tidal resource is assessed at three decadal length scales defined by the distance from the reference deployment at site 1:

- Macro-scale: distance greater than 1000 m (sites 2 and 3),
- Meso-scale: distance between 100 m and 1000 m (sites 4-6), and
- Micro-scale: distance less than 100 m (sites 7 and 8).

In an energetic environment, such as northern Admiralty Inlet, macro-scale variations are expected, but the magnitude of micro-scale gradients is difficult to predict *a priori*. For example, shipboard ADCP surveys of this site are able to identify meso-scale gradients, but cannot resolve micro-scale gradients [**13**].

Table 1 – Doppler profiler configuration for deployments in northern Admiralty Inlet, Puget Sound, WA

Site	Platform	Instrument	Deployment Dates (dd/mm/yy)	Duration (days)	Mean Depth (m)	Bin Size (m)	Sample Interval (s)	n_{sample} (m/s)	$n_{ensemble}$ (m/s)
1	SS #02	Nortek Continental 470 kHz	18/08/10 - 09/08/11	356	59	2	60	0.06	0.03
2	SS #01	RDI Workhorse 300 kHz	10/11/10 - 10/02/11	92	48	1	60	0.04	0.02
3	SS #01	RDI Workhorse 300 kHz	13/02/11 - 09/05/11	85	49	1	60	0.05	0.02
4	SS #03	Nortek AWAC 600 kHz	11/02/10 - 04/05/10	82	56	1	60	0.04	0.02
5	SS #03	Nortek AWAC 600 kHz	20/05/09 - 03/08/09	75	56	1	30	0.05	0.02
6	SS #04	Nortek AWAC 1 MHz	09/05/11 - 08/06/11	30	56	1	1	0.11	0.01
7	SS #03	Nortek AWAC 600 kHz	11/05/11 - 09/08/11	90	61	1	60	0.04	0.02
8	SS #04	Nortek AWAC 1 MHz	05/07/11 - 11/08/11	37	61	1	1	0.11	0.01

Four models of Doppler profilers were used over the course of the project: RDI Workhorse (300 kHz), Nortek Continental (470 kHz), and Nortek AWAC (600 kHz and 1 MHz). All units performed well, with near-100% data return for all deployments. The instrumented Sea Spider platforms are almost neutrally buoyant (-20 kg wet weight) and are ballasted by 360 kg of lead. This was sufficient to maintain instrument stability on the cobbled seabed. During a typical deployment, each tripod generally rotated by 25-50 degrees on the seabed during the first spring tide, but once established, did not experience further rotation[1].

2.2 Data Preparation

Measured currents were evaluated to exclude low quality data from results. First, measurements in the region shadowed by the water surface are excluded. Per [**14**], this region is approximately given by

$$H(1-\cos\phi), \tag{2.1}$$

where H is the water depth and ϕ is the angle between the ADCP transducer surface and vertical (20^o for RDI, 25^o for Nortek). For the deployments in Table 1, the observed shadow region varies between 4 and 6 m, consistent with (2.1) for water depths on the order of 60 m. Second,

[1]One deployment with SS #01 (300 kg of lead ballast) appears to have translated approximately 100 m from the as-deployed location, based on heading and pressure sensor logs and estimated as-recovered position. This deployment is not included in Table 1 or subsequent analysis, but serves to demonstrate the marginal stability of even low-drag platforms deployed in these types of energetic environments.

for measurements obtained with an RDI ADCP, bins with average correlation counts less than 60 are excluded. Nortek firmware automatically excludes measurements with comparably low correlation counts.

The sampling interval (i.e., the time between the start of each sample) varied by deployment, ranging from 1 s to 60 s. During most deployments with 60 s sampling intervals, the profilers collected information for 50-75% of the interval. In post-processing, all sampled velocities are converted to five minute ensembles ($\boldsymbol{U}_{\mathbf{ensemble}}$), filtering the majority of turbulent scale motion from the signal [**11**], while preserving the deterministic and meteorological components,

$$U_{\mathbf{ensemble}} = \overline{U_{\mathbf{sample}}} = \overline{U_{\mathrm{det}} + U_{\mathbf{met}} + U_{\mathbf{turb}} \pm n_{\mathbf{sample}}} \approx U_{\mathrm{det}} + U_{\mathbf{met}} \pm n_{\mathbf{ensemble}}, \qquad (2.2)$$

where the overbar denotes a temporal mean. This also reduces ensemble Doppler noise (n_{ensemble}) by a factor of $N^{1/2}$ relative the original Doppler noise (n_{sample}), where N is the number of samples in the ensemble. Consequently, all ensembles underpinning this analysis have a standard error less than 0.03 m s^{-1}. This is at least an order of magnitude smaller than the sum of the deterministic and meteorological components over all stages of the tide.

When the vertical velocity is small, it is convenient to describe the flow field in terms of horizontal velocity (U_h)

$$U_h = \pm\sqrt{u^2 + v^2} \qquad (2.3)$$

where, by convention, flood is signed positive and ebb is signed negative. This reduces the three dimensional flow field to a one dimensional time series. Principal component analysis [**15**] is used to determine the principal axes for ebb and flood.

Surface-gravity waves, including swell from the Strait of Juan de Fuca and locally generated wind-waves, have orbital velocities that decay with depth from the water surface. Here, wave-orbital velocities are not expected to affect sub-surface current resource metrics or turbine performance, because the depths of interests are more than half a wavelength beneath the surface. Moreover, the wave orbital velocities are obscured in calculating the five-minute ensembles used for resource metrics, because the orbital velocities (nominally 2-12 s period) have a zero Eulerian average on time scales longer than several wave periods (e.g., five minutes). At shallower sites, wave orbital velocities may contribute significant variance to the sub-surface velocity field, but zero-mean is still expected for all but the shallowest sites. To confirm these assertions, site-specific wave measurements were made from August to November 2010 using a 600 kHz AWAC deployed within several hundred meters of site 1. The AWAC recorded 1 Hz bursts of surface elevation and velocity for ten minutes at the top of each hour, from which the orbital velocities at depth are calculated using the wave frequency-directional spectra and linear finite-depth theory [**8**].

Tidal estuarine systems such as Puget Sound have sub-tidal exchange flows resulting from stratification. Here, these residual currents are evaluated using a low pass filter (PL66) [**16**]. A half-amplitude period of 40 hours is used; the tidal signal is not removed by shorter half-amplitude periods.

Storm surges that appreciably alter currents are uncommon in Puget Sound and none occurred during the data collection period. Similarly, given the expected deployment depth for hydrokinetic devices (e.g., > 5 m below the surface) and prevailing water depth (60 m), the signal from wind driven currents is negligible at this location.

2.3 Resource Characterization Metrics

A representative fortnight of ADCP data is shown in Figure 2. The magnitude and direction of the horizontal currents vary with time and vertical position. The tidal regime in northern Admiralty Inlet is characterized as mixed, mainly semidiurnal with two ebb and flood currents of unequal magnitude each lunar day.

Resource characterization metrics are used to compare locations. Only those characteristics with clear device performance or design implications are described here; a broader set are presented in [**12**].

Four time-averaged metrics are used to describe spatial variability:

- *Mean kinetic power density* [kW m^{-2}] – the time average of kinetic power density (K)
$$\overline{K} = \overline{\tfrac{1}{2}\rho\left|U_h^3\right|} \qquad (2.4)$$
where ρ is the density of seawater (nominally 1024 kg m^{-3}). The mean kinetic power density is equivalent to the mean flux of kinetic energy through a vertical plane, and this quantity is the first-order predictor of project economics [**17**].
- *Mean kinetic power asymmetry* [dimensionless] – the ratio of mean kinetic power density over all ebb currents to all flood currents, $\overline{K_{\text{ebb}}}/\overline{K_{\text{flood}}}$. This indicates whether power generation will be skewed towards one stage of the tide. Asymmetries may result from interactions between reflected tidal wavelengths (in an idealized embayment subjected to a single constituent harmonic forcing, peak ebb currents are slightly more intense than flood currents) or by local distortions to the harmonic currents caused by bathymetry and/or topography.
- *Peak velocity* [m s^{-1}] – the maximum horizontal velocity observed, $\max\left(\left|U_h\right|\right)$. Maximum currents are of interest for determining design loads. Here, the peak velocity associated with deterministic and meteorological currents are evaluated. Assessing the turbulent contribution to peak currents from ADCP data is problematic, even at high temporal resolution (e.g., 1 Hz), because Doppler uncertainty broadens the distribution of observed turbulence intensities, even for uniquely valued intensities [**18**]. In [**11**], a characteristic turbulent velocity fluctuation is defined, following the IEC standard for wind, however this is a statistical quantity and not equivalent to a peak turbulent velocity fluctuation.
- *Direction asymmetry* [degrees] – the asymmetry between the mean direction ($\bar{\theta}$) of ebb and flood, relative to bidirectional currents,
$$\overline{\theta_{\text{flood}}} - \overline{\theta_{\text{ebb}}} - 180^{\text{o}}. \qquad (2.5)$$

The performance of a fixed yaw turbine is degraded if the current direction and rotor plane are misaligned.

- *Direction standard deviation* [degrees] – the standard deviation of current direction relative to the principal axes (σ_θ). Around slack water, when turbines are idle, the reversing currents give rise to large, but irrelevant, direction deviations. The direction standard deviation is calculated only when the currents have fully set to ebb or flood, nominally $|U_h| \geq 0.5$ m s^{-1}. As for direction asymmetry, the performance of fixed yaw turbine is degraded if the current direction is misaligned with the rotor plane.

The *MATLAB* code to calculate these, and other metrics, is available for download at: http://depts.washington.edu/nnmrec/characterization. All measurement time series are available for download at: http://depts.washington.edu/nnmrec/project_meas.html.

2.4 Turbine Model

A simple model for the performance of a hydrokinetic turbine is used to assess the operational significance of variations in the tidal resource. The properties of an unshrouded horizontal axis tidal turbine representative of commercial prototypes are presented in Table 2. Inflow conditions over the turbine rotor are approximated by hub-height values and the device power output (P) is described as a function of horizontal velocity by

$$\begin{aligned} P &= 0 && \left|U_h \cos^{1/3}\gamma\right| < U_{\text{cut-in}} \\ P &= \tfrac{1}{2}\rho |U_h|^3 \cos^2\gamma \left(\frac{\pi D^2}{4}\right)\eta_p \eta_e && U_{\text{cut-in}} \leq \left|U_h \cos^{1/3}\gamma\right| \leq U_{\text{rated}} \\ P &= \tfrac{1}{2}\rho U_{\text{rated}}{}^3 \left(\frac{\pi D^2}{4}\right)\eta_p \eta_e && \left|U_h \cos^{1/3}\gamma\right| > U_{\text{rated}} \end{aligned} \qquad (2.6)$$

where γ is the angle between the current and rotor plane (γ=0 when flow is aligned with the rotor plane), D is the turbine diameter (and thus $\pi D^2/4$ is the swept area of the turbine), η_p is the performance coefficient of the rotor, η_e is the efficiency of the power train (gearbox, generator, power electronics), $U_{\text{cut-in}}$ is the speed at which the turbine begins to rotate, and U_{rated} is the speed at which maximum power is generated (beyond this point, power extraction is curtailed through active pitch control or dynamic stall). For simplicity, the performance coefficient and power train efficiency are idealized as constant over the full range of operating conditions.

A number of commercial prototype tidal turbines are fixed yaw devices [**19**, Section 2] and cannot respond to directional fluctuations. The effect of rotor misalignment is captured, to the first order, as a $\cos^2\gamma$ reduction in power generated [**20,21**]. This is a combination of decreases in the apparent turbine swept area and in the relative inflow velocity, as reflected by the $\cos^{1/3}\gamma$ terms in (Eq. 2.6) [**20**]. For a passively yawed turbine, it is assumed that γ is always equal to zero. For a fixed yaw turbine, the alignment angle that maximizes average power generation is determined iteratively. The rated speed is chosen to yield economically viable capacity factors (e.g., 30%) in a mixed, mainly semidiurnal tidal regime [**17**]. It is assumed that energy removal

will not appreciably alter inflow conditions (e.g., average power extracted by a single device is much less than the theoretical resource limit; [**22**]) and that blockage effects are negligible [**23**] given the dissimilar magnitudes of turbine swept area (~10^2 m^2) to channel cross-sectional area (~10^5 m^2).

Table 2 – Horizontal axis turbine parameters

Parameter	Value
Rotor diameter (D)	25 m
Hub height	Mid-water depth (~30 m above seabed)
Performance coefficient (η_p)	50%
Power train efficiency (η_e)	90%
Cut-in speed ($U_{cut\text{-}in}$)	0.7 m s^{-1}
Rated speed (U_{rated})	2.25 m s^{-1}
Rated power	1.3 MW

2.5 Performance Characterization Metrics

Performance metrics used for this analysis include:

- *Mean power* [MW] – the time average of power output (P). This is proportional, conceptually, to project revenue.
- *Capacity factor* [%] – the ratio of average power to rated power. This is an indicator of the degree of capital utilization for a project.
- *Percentage of time operating* [%] – the percentage of time the turbine is operating (sometimes referred to as exceedence). This is helpful to understanding the persistence of environmental stressors such as dynamic effects (i.e., rotating blade), noise, and electromagnetic fields [**24**].

As is standard in the wind industry, rather than directly calculating power generation from an underlying time series, the data are reduced to a joint probability distribution of horizontal velocity (U_h) with direction (θ). Note that the joint probability distribution retains the relationship between velocity and direction, as opposed to independent probabilities distributions of each, and this is essential to correctly evaluate power output (Eq. 2.6). Horizontal velocity magnitude and direction discretization to 0.1 m s^{-1} and 1^o result in biases of less than 1% for mean power generation estimates relative to direct calculation (not shown).

2.6 Metric Uncertainty

Metrics calculated from finite-length observations may diverge from their true values (defined as the average over an infinite observation). Generically, the convergence of a metric to its true value is given by

$$\frac{\int_0^T M(t)dt \Big/ \int_0^T dt}{\int_0^\infty M(t)dt \Big/ \int_0^\infty dt}, \qquad (2.7)$$

where $M(t)$ is the time varying metric and T is the length of observation. In shorthand, the averaging time for a metric is represented with a superscript and posited to have converged when

$M^T \approx M^\infty$. Since M^∞ is not known a priori, this convergence can only be investigated in a proximate manner for a measured velocity consisting of deterministic, meteorological, and turbulent components. However, for the harmonic component, the value of a metric calculated over the tidal epoch (18.6 years) is likely to approach its true value (i.e., $M^{\text{epoch}} \approx M^\infty$). Because the aharmonic component is a non-linear response to the harmonic component, the deterministic currents should converge at a similar rate to the harmonic component. Further, if the meteorological currents are weak, convergence of the harmonic component may be a reasonable proxy for convergence of measured currents.

The *MATLAB T_TIDE* routine [**25**] is used to extract harmonic constituents from the horizontal velocity observations at mid-water from site 1. The Rayleigh criterion is slightly relaxed to 0.97, resulting in 60 constituents that are significant at 95% confidence level. A predicted time series over the tidal epoch is generated. Over longer time scales (days to years), the beating between constituents gives rise to decaying oscillations in the calculated metrics with periodicity,

$$T_{\text{beat}} = \frac{1}{(f_1 - f_2)}. \tag{2.8}$$

For example, the beating between the principal lunar semidiurnal constituent (M2) and principal solar semidiurnal constituent (S2) gives rise to the well-known 14.8 day neap-spring cycle. Because the modulation amplitude depends on the relative amplitude of the beating constituents, the results presented here may only be applicable to mixed, mainly semi-diurnal tidal regimes.

From the epoch prediction for horizontal velocity, a series of 185 day records are extracted at a time resolution of 15 minutes, each offset by 20 days (no constituent beating at this frequency). This yields 336 realizations of harmonic currents over the epoch. For each realization, the rate of convergence for three metrics is evaluated:

- mean kinetic power density: $\overline{K^T_{\text{harmonic}}} \Big/ \overline{K^{\text{epoch}}_{\text{harmonic}}}$,
- maximum velocity: $\max\left(U^T_{h,\text{harmonic}}\right) \Big/ \max\left(U^{\text{epoch}}_{h,\text{harmonic}}\right)$, and
- mean power generation: $\overline{P^T_{\text{harmonic}}} \Big/ \overline{P^{\text{epoch}}_{\text{harmonic}}}$.

Figure 3 shows the convergence of mean power density, calculated from harmonic currents, to its epoch value. Given that the neap-spring cycle is the dominant beating between constituents at this location, it is unsurprising that the standard error decreases to 5% after two complete cycles (30 days). The standard error then continues a gradual, oscillatory decay, declining to 2% after 160 days. For the purpose of characterizing mean power density, a record length of 30 days, or longer than 70 days, provides 5% accuracy. When the temporal mean contains less than an integer number of beat periods (Eq. 2.8), the calculated metric will deviate from its true value. While all finite-length records, by definition, contain a non-integer number of constituent beat periods, as the record length increases the associated bias declines. For example, the local maximum in standard error at 38 days corresponds to a record length of 2.5 neap-spring cycles, where the relative position in the cycle is likely to bias the metric high or low. By 180 days, the

neap-spring oscillations are less pronounced, as a consequence of the record encompassing more than a dozen beat periods. A synthetic tidal series containing only the M2 and S2 constituent (and, therefore, only a neap-spring beating) would have zero standard error for record lengths containing an integer number of beat frequencies.

As shown in Figure 4, the probability of observing the maximum harmonic currents over the tidal epoch within a finite observation period is low, even for observations exceeding half a year. For example, after 6 months, the probability of having observed the 95^{th} percentile harmonic currents is less than 0.8, which is insufficient to directly inform device design. For the more typical site characterization field study lasting 30 days, the probability of having observed the 95^{th} percentile harmonic currents is less than 0.25. This motivates statistical projections of peak velocity for device design, since direct observation is difficult.

Figure 5 shows the convergence of mean power generation, calculated from harmonic currents, to its epoch value. Convergence is qualitatively similar to mean power density, but mean power generation converges more rapidly to its epoch value than the mean power density because of the non-linear damping caused by power shed above rated speed (Eq. 2.6). The standard error decreases to within 3% of its epoch value at 30 days and to within 2% after 160 days.

3 Results

3.1 Contribution of Meteorological Currents

Analysis of AWAC wave data (August to November, 2010) indicates that surface-gravity waves in the vicinity of Admiralty Head are typically local wind-waves, with significant wave heights < 1 m and dominant periods < 4 s. According to linear finite-depth theory [**8**], the associated wave orbital velocities will decay to 0.1 m s^{-1} at depths of 5 m below the surface. Under the maximum observed wave conditions of 2.3 m significant wave height and 6.7 dominant period, the wave orbital velocities are 0.4 m s^{-1} at a depth of 5 m below the surface and 0.1 m s^{-1} at depth of 20 m below the surface. Again, these velocities are obscured (zero mean) in the five-minute ensembles, similar to the turbulent fluctuations.

Residual currents at site 1 are presented in Figure 6 and are representative of those over the study area. A classical circulation pattern is observed, with net outflow near the surface and net inflow near the seabed. There is also a seasonal variation, with relative maxima in the early summer (snow melt freshet) and the late fall (precipitation from strong storms). Because strong tidal exchanges over the Admiralty Inlet sill mix the water column, residual currents are strongest during neap tides and weakest during spring tides. At mid-water (30 m from seabed), residual currents are ubiquitously weak, with a maximum amplitude rarely exceeding 0.1 m s^{-1}. Closer to the seabed and surface, residual currents are more intense, approaching 0.4 m s^{-1}. Observations do not indicate measurable wind-driven currents or storm surge currents, consistent with expectations for this location.

The relative contribution of deterministic and meteorological currents to the measured currents, therefore, varies with depth. Over all depths, the peak deterministic (tidal) currents are nearly an order of magnitude more intense than the meteorological currents. Residual currents are

significant near the surface and seabed, but not over the middle of the water column. Within 5 m of the surface, wave orbital velocities are of similar order to residual currents, but are insignificant over most of the water column.

3.2 Temporal and Spatial Variability in the Tidal Resource

Building on the analysis of metric uncertainty for the harmonic component of measured velocity (Section 2.6), the temporal variability and, therefore, uncertainty, in all resource metrics is evaluated using mid-water data from site 1. While this is a finite-length observation, the dominant periodicities are well-represented in the year-long time series. Convergence is shown in Figure 7 for power density, direction, and maximum velocity. Mean power density and power density asymmetry converge in a manner consistent with the previous analysis of the harmonic component, providing support for the assumption that the deterministic (harmonic and aharmonic) and harmonic contributions to resource metrics converge at similar rates. Direction convergence (asymmetry and variation) appears to require longer observation times. This is counterintuitive, given that there should not be a fundamental periodicity to tidal direction. However, because a flux gate compass is only accurate to a few degrees, the variations shown in Figure 7 are more likely attributable to sensor drift. The convergence of maximum velocity offers a cautionary example for resource characterization. While this metric appears to converge rapidly to its true value, analysis of harmonic currents suggests that it is unlikely for $\max\left(U_h^{1\,\text{year}}\right) \approx \max\left(U_h^{\infty}\right)$. Therefore, observed maximum velocity is likely to be lower than its true value and is reported only to demonstrate the strength of measured tidal currents at this site.

Spatial variability is discussed in the context of three decadal length scales defined by the distance from the reference location (site 1): micro-scale for less than 100 m separation, meso-scale for 100 m to 1000 m, and macro-scale for more than 1000 m. Resource characteristics for all locations are tabulated in Table 3 at mid-water depth. The observed macro-scale resource variations are expected given that site 2 is to the lee of the headland and site 3 is close to the channel center, away from the headland influence. Applying a 1 kW m^{-2} threshold for an economically attractive mean power density [**17**], sites 1 and 3 are candidates for tidal energy development, but site 2 is not, being close enough to the headland to be within the flood eddy[2]. Over meso-scale distances (sites 4-6) and micro-scale distances (sites 7-8), all sites have potential for development, but variations in power and direction metrics exceed metric uncertainty. The micro-scale variations are of particular interest for site development. For example, the mean power density at Site 7 is more than 10% higher than at Site 1, even though the two sites are separated by only 60 m and resource properties are evaluated at nearly the same absolute depth.

The bias in current strength towards ebb at sites 1 and 4-8 is likely to result from flow acceleration around the nearby headland and the separation that occurs in its lee [**26**]. Admiralty

[2] The objective of this deployment was to gather information about harbor porpoise response to passenger ferry operation. This location was never considered a likely candidate for tidal energy development and is included in this discussion to illustrate macro-scale variations in mean kinetic power density.

Head has a length (alongshore) of 5.5 km and width (offshore) of 2.5 km. The mean depth in the near-shore area is approximately 30m. On a strong ebb, horizontal currents exceed 2.5 m/s and are dominantly semi-diurnal. Per the scaling arguments presented in [**27**], these translate to length scales for frictional dissipation and the tidal excursion of 6 km and 35 km, respectively. For these values, eddy propagation would be expected to be similar to steady flow, with a characteristic eddy size comparable to the characteristic size of the headland.

Table 3 – Resource characteristics at sites in northern Admiralty Inlet, Puget Sound, WA

Site	Distance to Site 1 (km)	Distance from Seabed (m)	Mean kinetic power density[1] (kW m^{-2})	Mean kinetic power asymmetry	Directional asymmetry (degrees)	Directional variation (degrees)	Maximum velocity[2] (m/s)
1	-	30	1.8 ± 0.04	1.6	24	10	3.4
2	1.10	24	0.6 ± 0.02	7.8	8	12	2.5
3	2.60	24	1.4 ± 0.06	0.9	8	7	3.1
4	0.35	28	1.7 ± 0.07	1.0	27	11	3.0
5	0.23	28	2.1 ± 0.09	1.1	23	10	3.4
6	0.19	28	2.0 ± 0.10	1.2	23	9	3.3
7	0.06	31	2.0 ± 0.08	1.6	20	9	3.4
8[3]	0.07	31	2.0 ± 0.10	1.7	19	9	3.1

[1] Standard error based on analysis of harmonic velocity (Figure 3).
[2] These are likely to be understated relative to their true values for all sites given the duration of observation.
[3] Time series truncated to 30 days so that metric uncertainty is similar to other locations surveyed.

Variations with depth for a selection of sites representing macro-, meso-, and micro-scales relative to the reference site are presented in Figure 8. The vertical coordinate is normalized by the total water depth (H). In general, mean power density increases towards the surface, as would be expected assuming a no-slip condition at the seabed and a classic bottom boundary layer. For sites near the headland, the ebb power density is nearly twice that of flood near the seabed, but ebb and flood approach parity near the surface. Conversely, the direction asymmetry increases with distance from the seabed, exceeding 20 degrees for locations near the reference site. Direction variation uniformly reaches a minimum at mid-water. As for the mid-water results presented in Table 3, comparable variations are observed over micro and meso-scales at all depths.

3.3 Temporal and Spatial Variability in Turbine Performance

Spatial variability in turbine performance is evaluated using the simple turbine model described in Section 2.4. The uncertainty in performance metrics is investigated in a similar manner to resource characterization metrics using the long-term data from site 1. Figure 9 shows the convergence of performance metrics at this location to their 1-year values. As with resource metrics, convergence is in general agreement with the analysis of the harmonic component. The damping in power resulting from the rated speed is apparent, with a more rapid convergence to long-term values than for the resource characteristics. Because the operating percentage is affected in a non-linear manner by the cut-in speed (rather than rated speed), this metric converges in a different manner than mean power generation.

Table 4 shows performance metrics at difference sites for devices with mid-water hub heights. Spatial variability mirrors the trends in resource characteristics. Variability on a macro-scale is

pronounced, with mean power generation at sites 2 and 3 only 30% and 80% of the site 1 value. Over meso- and micro-scales, average power generation varies by 5-10% from the reference site. This exceeds measurement uncertainty and is operationally significant in terms of cost of energy, suggesting an economic benefit to micro-siting.

Operating time for devices with economically attractive capacity factors exceeds 70% at most locations. From an ecological standpoint, the stressors associated with turbine operation would be present for the majority of time, but not continuous. The operating time is strongly dependent on the device cut-in speed.

Performance differences between passive yaw and fixed yaw turbines are also presented in Table 4. The effect of off-axis flow is a function of direction asymmetry, direction variation, and power density asymmetry (e.g., the effect of direction asymmetry is muted if there is also a large power density asymmetry between ebb and flood). For sites at mid-water near the headland, the mean power generation for a fixed yaw device is, at most, 5% lower than for a passive yaw device. This may be operationally significant, but economically offset by reduced device complexity for fixed yaw turbines. As shown in Figure 10, near the seabed, the penalty for a fixed yaw device slightly increases, with higher direction variation (σ_θ) dominating over lower direction asymmetry.

Table 4 – Turbine performance at sites in northern Admiralty Inlet, Puget Sound, WA

			Passive Yaw			Fixed Yaw		
Site	**Distance to Site 1 (km)**	**Turbine Depth (m)**	**Average power output (MW)**	**Capacity factor (%)**	**Time operating (%)**	**Average power output (MW)**	**Capacity factor (%)**	**Time operating (%)**
1	0	30	0.35	28%	72%	0.34	26%	72%
2	1.07	24	0.12	9%	36%	0.12	9%	36%
3	2.59	24	0.29	22%	66%	0.28	22%	66%
4	0.4	28	0.35	27%	76%	0.33	26%	76%
5	0.2	28	0.39	30%	73%	0.37	29%	73%
6	0.19	28	0.38	30%	76%	0.36	28%	76%
7	0.06	31	0.38	29%	74%	0.36	28%	74%
8	0.07	31	0.39	30%	75%	0.38	29%	75%

4 Discussion

Operationally significant variations in the tidal resource (5-10% variations in mean power generation) are identified over length scales less than 100 m (micro-scale variations). This has several consequences for resource characterization activities. First, variations on these length scales are unlikely to be resolved by shipboard surveys [**13**,**28**], though such approaches are useful for mapping larger-scale variability. Second, if numerical models are used to resolve micro-scale gradients, grid resolution should be O(10 m). The magnitude of the observed micro-scale gradients may be somewhat unique to this site given the proximity to a headland (Admiralty Head at less than < 1 km). Site developers will need to balance the beneficial resource intensification around headlands against micro-siting difficulties and ebb/flood asymmetries. Because of these asymmetries at headland sites, passive/active yaw turbines are

expected to produce somewhat more power than fixed yaw turbines (at most 5% for this location).

The resource metrics presented here emphasize power density over velocity. Device performance varies with the power density (velocity cubed), so mean velocity is not an inherently useful metric for tidal resource characterization. The root mean cubed velocity can be directly converted to mean power density, but can cause confusion if not carefully defined by practitioners. For mixed, mainly semidiurnal tidal energy sites, the cumulative probability density functions (CPDF) of velocity and power density are also illuminating. As shown in Figure 11, approximately 50% of the power density (and, therefore, possible power generation) occurs at velocities greater than 2 m/s. However, these velocities occur only 10% of the time.

These results also provide insight into data collection strategies informing device siting decisions, estimate performance, and determine design loads. For all performance metrics (and resource metrics related to performance) reasonable accuracy (i.e., standard error of 5%) is obtained from 30-day observations. In fact, the beating of harmonic constituents increases uncertainty in metrics calculated from data collected over marginally longer periods (i.e., 30 – 50 days). For mixed, mainly semidiurnal sites, survey periods of less than 30 days are not recommended. When the dominant velocity components are deterministic and turbulent, sampling over 30 days at a rate of 1 Hz can provide useful information about resource characteristics, device performance, and turbulent motions [**11**]. This type of data collection is within the capabilities of the current generation of Doppler profilers when equipped with GB-capacity storage cards and lithium-ion batteries. However, if the meteorological component is appreciable, longer-term data collection may be necessary to estimate device performance.

The assessment of design loads is more problematic. Specifically, the probability of observing the 90^{th} percentile tidal epoch velocity within a 30 day period is only slightly more than 50%. Since operational lifetimes for devices are on the same order as the tidal epoch (i.e., 20 years), maximum observed currents should not be taken as a proxy for maximum expected currents over the device design lifetime. How best then to estimate design loads without resorting to extreme factors of safety? One approach is to rely on harmonic analysis to predict the deterministic component and treat turbulent and meteorological currents statistically. This is, however, problematic for three reasons. First, if the deterministic currents contain a strong aharmonic component, this will not be captured by harmonic analysis and predicted velocities may substantially under- or over-predict maximum deterministic currents. Second, accurate prediction of currents over the tidal epoch requires at least a year of data, which may be an onerous cost burden for site developers. While inference from a reference station [**5**] may overcome this difficulty, preliminary analysis of tidal elevation and current constituents from this site suggest that amplitude ratios and phase differences for currents should not be assumed, without verification, to be equivalent to those of the tidal elevation constituents. Third, conventional harmonic analysis is only suitable for predicting both magnitude and direction when currents progress through an ellipse [**5**], which is not always the case at energetic sites. Given the number

of prototype tidal turbine failures ascribed to under-estimation of design loads, there remains a clear need to develop rigorous techniques for determining maximum design velocities.

5 Conclusions

This paper presents multi-year observations of tidal currents at a proposed tidal energy site in Admiralty Inlet, Puget Sound, WA (USA). Both the spatial variability in the tidal resource and the implications for device performance are evaluated. Resource and performance metrics are proposed that intuitively reduce the observational data for decision making purposes. These metrics show that operationally significant variations in turbine performance are likely over length scales on the order of 100 m. This has important implications for the arrangement of turbines within an array, particularly at locations close to headlands.

6 References

1 Arbic, B. and **Garrett, C.** A coupled oscillator model of shelf and ocean tides. *Continental Shelf Research*, 2010, **30**(6), 564-574.

2 Teledyne RD Instruments *Acoustic Doppler current profiler principles of operation: A practical primer*, 2006, Poway, CA: Teledyne. RDI P/N 951-6069-00.

3 Brumley, B.H., Cabrera, R.G., Deines, K.L, and **Terray, E.A.** Performance of a Broad-Band Acoustic Doppler Current Profiler, *IEEE Journal of Oceanic Engineering*, 1991, **16**(4), 402-407.

4 Godin, G. On the predictability of currents, *International Hydrographic Review*, 1983, **60**, 119-126.

5 Foreman, M.G., Crawford, W.R., and **Marsden, R.F.** De-tiding: theory and practice, *Quantitative Skill Assessment for Coastal Ocean Models, Coastal and Estuarine Studies*, 1995, **47**, 203-239.

6 Polagye, B., Epler, J. and **Thomson, J.** Limits to the predictability of tidal current energy, *MTS/IEEE Oceans 2010*, Seattle, WA, 20-23 September 2010.

7 Wang, D. Wind-driven circulation in the Chesapeake Bay, Winter 1975. *J. Physical Oceanography*, 1979, **9**, 564-572.

8 Mei, C.C. *The Applied Dynamics of Ocean Surface Waves*, 1989, World Scientific, Singapore.

9 Hansen, D.V. and **Rattray, M.** Gravitational circulation in straits and estuaries, *J. Marine Research*, 1966, **23**(2), 104-121.

10 Pugh, D.T. Tides, surges, and mean sea-level, 1987, 472 pp., J. Wiley, Chichester.

11 Thomson, J., Polagye, B., Durgesh, V., and **Richmond, M.** Measurements of turbulence at two tidal energy sites in Puget Sound, WA (USA), *IEEE J. Ocean. Eng.*, 2012, 37(3):363-374.

12 Gooch, S., Thomson, J., Polagye, B., and **Meggitt, D.** Site characterization for tidal power, *MTS/IEEE Oceans 2009*, Biloxi, MI, 26-29 October 2009.

13 Epler, J., Polagye, B., and **Thomson, J.** Shipboard acoustic Doppler current profiler surveys to assess tidal current resources, *MTS/IEEE Oceans 2010*, Seattle, WA, 20-23 September 2010.

14 Brown, J., Barton, E.D., Trasvina, A., Velez, H.S., Kosro, P.M., and **Smith, R.L.** Estimation of surface winds from upward looking acoustic Doppler current profilers, *J. Geophys. Res.*, 1992, **97**, 17925-17930.

15 Emery, W. J. and **Thomson, R.E.** Data analysis methods in physical oceanography, 2001, 638 pp., Elsevier, Amsterdam.

16 Beardsley, R., Limeburner, R., and **Rosenfeld, L.** CODE-2: moored array and large-scale data report, *Woods Hole Oceanographic Institute Technical Report WHOI-85-35*, 1985, 21 pp., Woods Hole Oceanographic Institute, MA.

17 Bedard, R., Previsic, M., Polagye, B., Hagerman, G., and **Casavant, A.** North America tidal in-stream energy conversion technology feasibility study, *EPRI TP-008-NA*, 2006, 9 pp., Electrical Power Research Institute, CA.

18 Polagye, B. and **Thomson, J.** Noise removal from Doppler profiler measurements of turbulence, *Submitted to IEEE J. Ocean. Eng.*

19 Polagye, B., Van Cleve, B., Copping, A., and **Kirkendall, K.** (eds) Environmental effects of tidal energy development, *NMFS F/SPO-116*, 2011, NOAA, U.S. Dept. Commerce, MD, 186 pp.

20 Pedersen, T.F. On wind turbine power performance measurements at inclined airflow, *Wind Energ*, 2004, **7**:163–176 (DOI: 10.1002/we.112)

21 Bahaj, A.S., Molland, A.F., Chaplin, J.R., and **Batten, W.M.J.** Power and thrust measurements of marine current turbines under various hydrodynamic flow conditions in a cavitation tunnel and a towing tank, *Renewable Energy*, 2007, **32**:407-426.

22 Garrett, C. and **Cummins, P.** The power potential of tidal currents in channels, *Proc. R. Soc. A*, 2005, doi:10.1098/rspa.2005.1494.

23 Garrett, C. and **Cummins, P.** The efficiency of a turbine in a tidal channel, *J. Fluid. Mech*, 2007, **588**, doi:10.1017/S0022112007007781.

24 **Boehlert, G.W.** and **Gill, A.B.** Environmental and ecological effects of ocean renewable energy development: a current synthesis, *Oceanography*, 2010, **23**(2), 68-81.

25 Pawlowicz, R., Beardsley, R. and **Lentz, S.** Classical tidal harmonic analysis including error estimates in MATLAB using T_TIDE, *Computers & Geosciences*, 2002, **28**(8), 929-937.

26 Geyer, W.R, and **Signell, R.P.** Measurements of tidal flow around a headland with a shipboard acoustic Doppler current profiler, *J. Geophys. Res.*, 1990, **95**(C3), 3189-3197.

27 Signell, R.P. and **Geyer, W.R.** Transient eddy formation around headlands, *J. Geophys. Res.*, 1991, **96**(C2), 2561–2575.

28 Palodichuk, M., Polagye, B., and **Thomson, J.** Resolving Spatial Resource Gradients at Tidal Energy Sites, , *In revision with IEEE J. Ocean Eng.*

7 Acknowledgements

The authors would like to thank Joe Talbert, Jeff Epler, Chris Bassett, Sam Gooch, and Capt. Andy Reay-Ellers for their assistance in collecting these data. Thanks also to Bob Thresher at

NREL for discussions around the appropriate treatment of off-axis flows for fixed and passive yaw turbines.

8 Funding Acknowledgement

Funding for this study is provided by the United States Department of Energy and Snohomish Public Utility District [DE-FG36-08GO18179]. This report was prepared as an account of work sponsored by an agency of the United States Government. Neither the United States Government nor any agency thereof, nor any of their employees, makes any warranty, expressed or implied, or assumes any legal liability or responsibility for the accuracy, completeness, or usefulness of any information, apparatus, product, or process disclosed, or represents that is use would not infringe privately owned rights. Reference herein to any specific commercial product, process, or service by trade name, trademark, manufacturer, or otherwise does not necessarily constitute or imply its endorsement, recommendation, or favoring by the United States Government or any agency thereof. Their views and opinions of the authors expressed herein do not necessarily state or reflect those of the United States Government or any agency thereof.

9 List of Figure Captions

Figure 1 – ADCP deployment locations superimposed on bathymetry: (left) reference site (1: 48.1530 N, 122.6880 W) and macro-scale comparison sites (2,3), (right) reference site (2) and meso- and micro-scale comparison sites (4-8). All distances are referenced to Site 1. Admiralty Head is directly to the east of the site.

Figure 2 – Representative ADCP data (days 0-15 from Site 5): (top) Horizontal velocity magnitude, (bottom) horizontal velocity direction.

Figure 3 – (top) Convergence of mean power density (calculated from harmonic currents) to its epoch value. Thin lines denote individual realizations over the epoch. Dashed lines denote standard error. (bottom) Standard error normalized by running mean power density as a function of observation time.

Figure 4 – (top) Convergence of the maximum harmonic current to its epoch value. Thin lines denote individual realizations over the epoch. (bottom) Probability of observing the N^{th} percentile harmonic currents over a given observation time.

Figure 5 – (top) Convergence of average power generation (calculated from harmonic currents) to its epoch value. Thin lines denote individual realizations over the epoch. Dashed lines denote standard error. (bottom) Standard error normalized by running mean of power generation as a function of observation time.

Figure 6 – Residual currents for Site 1. Gaps in the record correspond to recovery and redeployment of the instrumentation package.

Figure 7 - Convergence of resource metrics to annual average values (site 1): power density (top), mean direction (middle), and maximum velocity (bottom).

Figure 8 – Vertical variations in resource characteristics at sites in northern Admiralty Inlet, Puget Sound, WA. Acoustic interference over dashed portion of reference site profiles.

Figure 9 – Convergence of turbine performance metrics to long-term values (Site 1, passive yaw).

Figure 10 – Vertical profiles of average power generation for a turbine (site 7), contrasting performance between passive and fixed yaw devices over a range of depths.

Figure 11 – Cumulative probability density functions of velocity and power density (site 1, mid-water depth).

10 List of Notation

D	turbine diameter (m)
η_p	rotor performance coefficient
η_e	power train efficiency
H	water depth (m)
γ	angle between the current and rotor plane (degrees)
K	kinetic power density (kW m^{-2})
M	a time varying metric describing the tidal resource or device performance
$n_{ensemble}$	Doppler uncertainty in ensemble average currents (m s^{-1})
n_{sample}	Doppler uncertainty in measured currents (m s^{-1})
P	device power output (kW)
φ	angle between Doppler profiler transducer surface and vertical (degrees)
ρ	seawater density (kg m^{-3})
σ_θ	standard deviation of current direction (degrees)
θ	direction of current (degrees)
$U_{cut\text{-}in}$	the speed at which a device begins to generate power (m s^{-1})
$\boldsymbol{U_{det}}$	deterministic component of tidal currents (m s^{-1})
$\boldsymbol{U_{ensemble}}$	ensemble average currents (m s^{-1})
U_h	horizontal velocity, vector sum of north and east components (m s^{-1})
$\boldsymbol{U_{met}}$	meteorological component of tidal currents (m s^{-1})
U_{rated}	the speed at which maximum power is generated by a device (m s^{-1})
$\boldsymbol{U_{turb}}$	turbulent component of tidal currents (m s^{-1})
$\boldsymbol{U_{sample}}$	measured currents (m s^{-1})

Subscripts and superscripts

overbar	time average
ebb	ebb tidal currents (seaward direction)
flood	flood tidal currents (landward direction)

T	length of a finite observation
∞	an infinite observation
epoch	an observation over the tidal epoch (18.6 years)
harmonic	the harmonic component of the deterministic tidal current

Figure1
Click here to download high resolution image

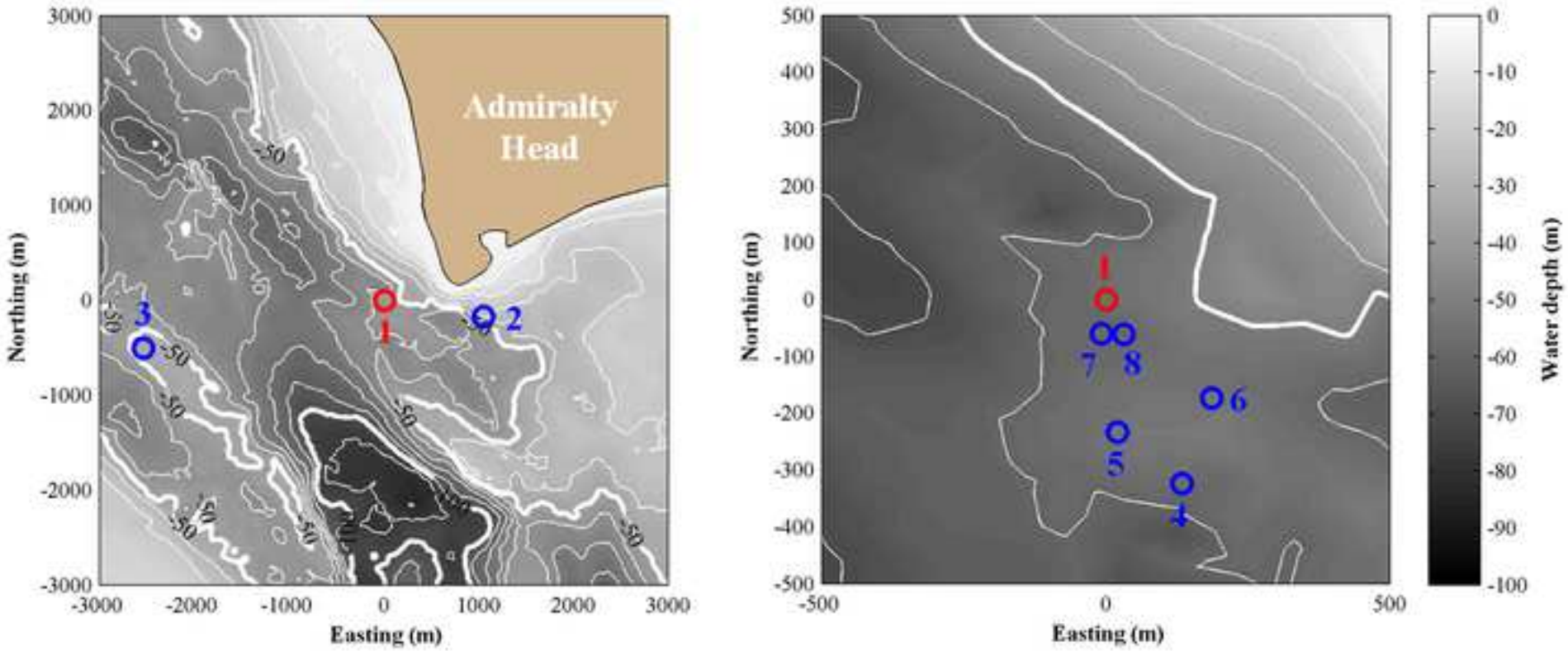

Figure2
Click here to download high resolution image

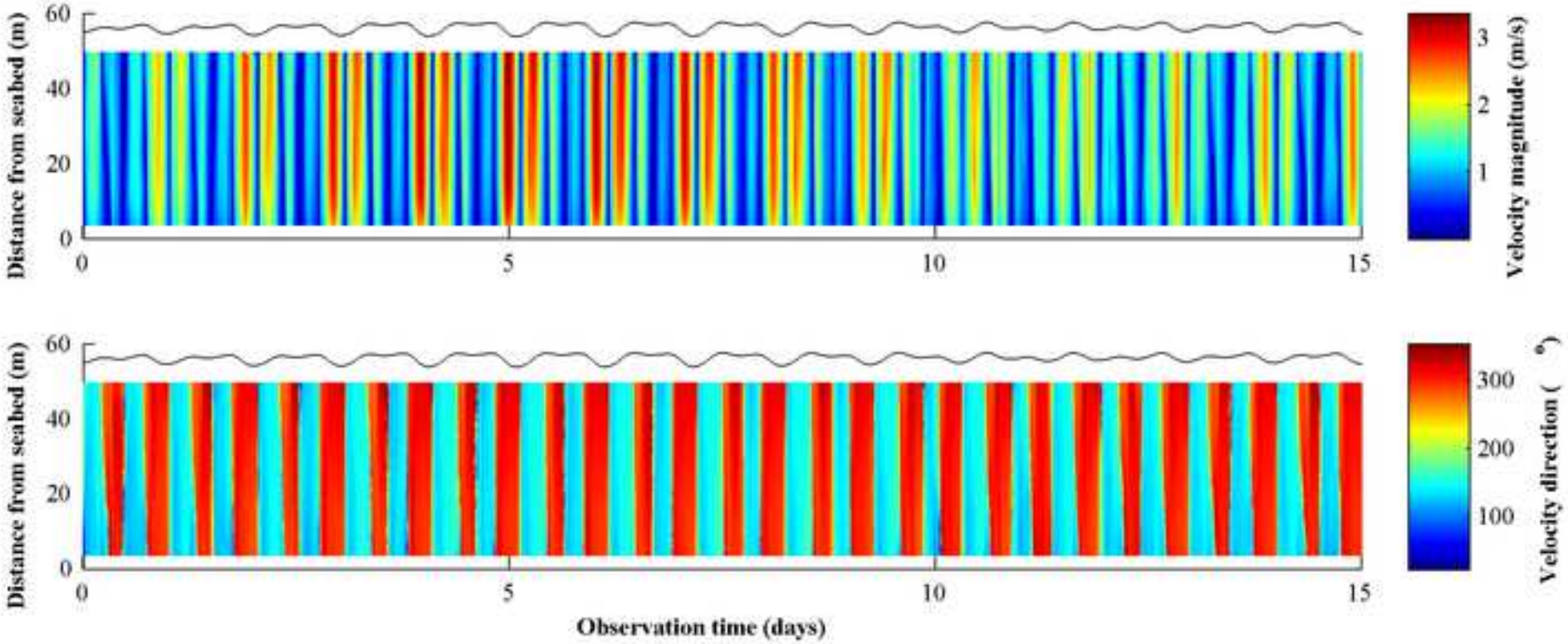

Figure3
Click here to download high resolution image

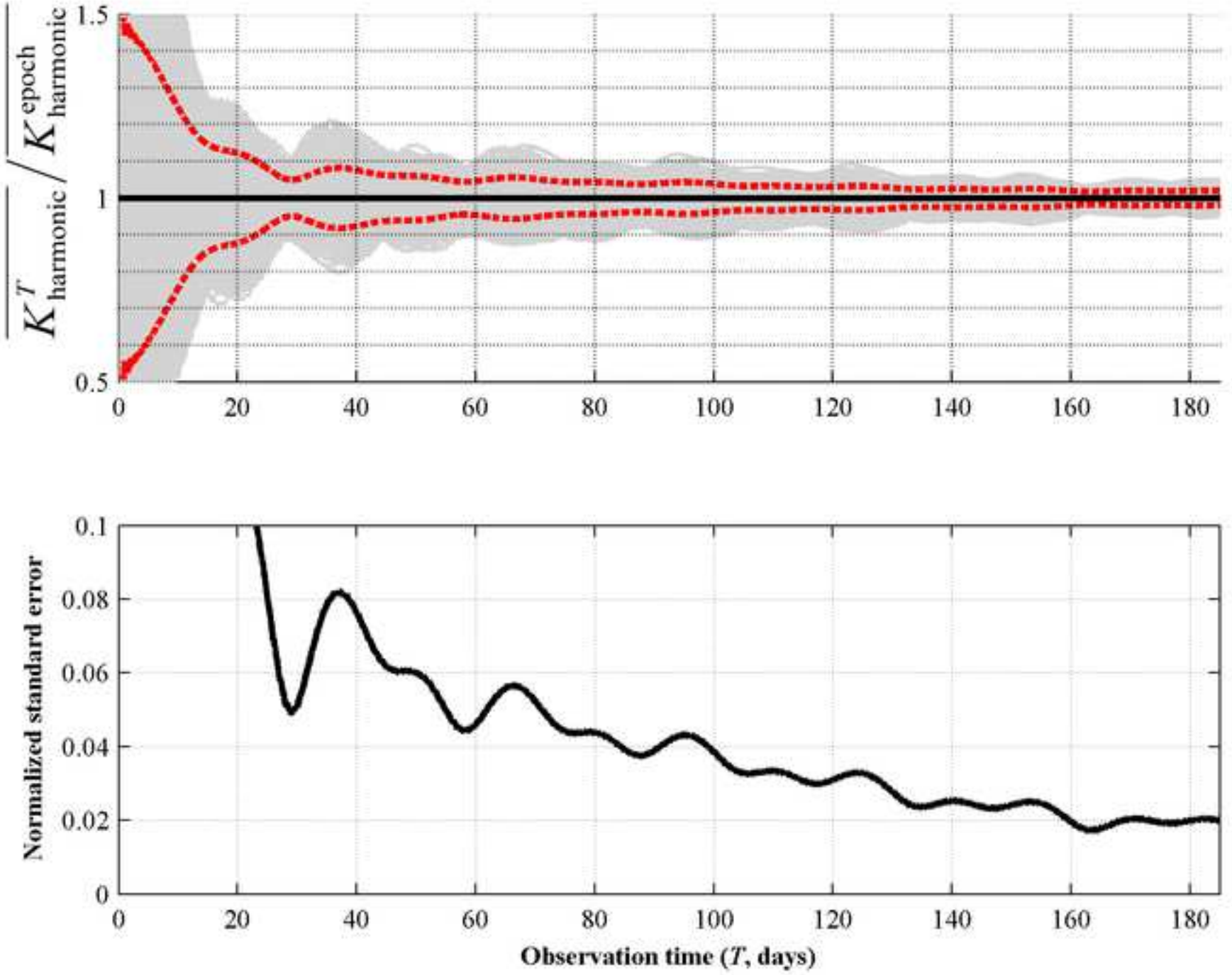

Figure4
Click here to download high resolution image

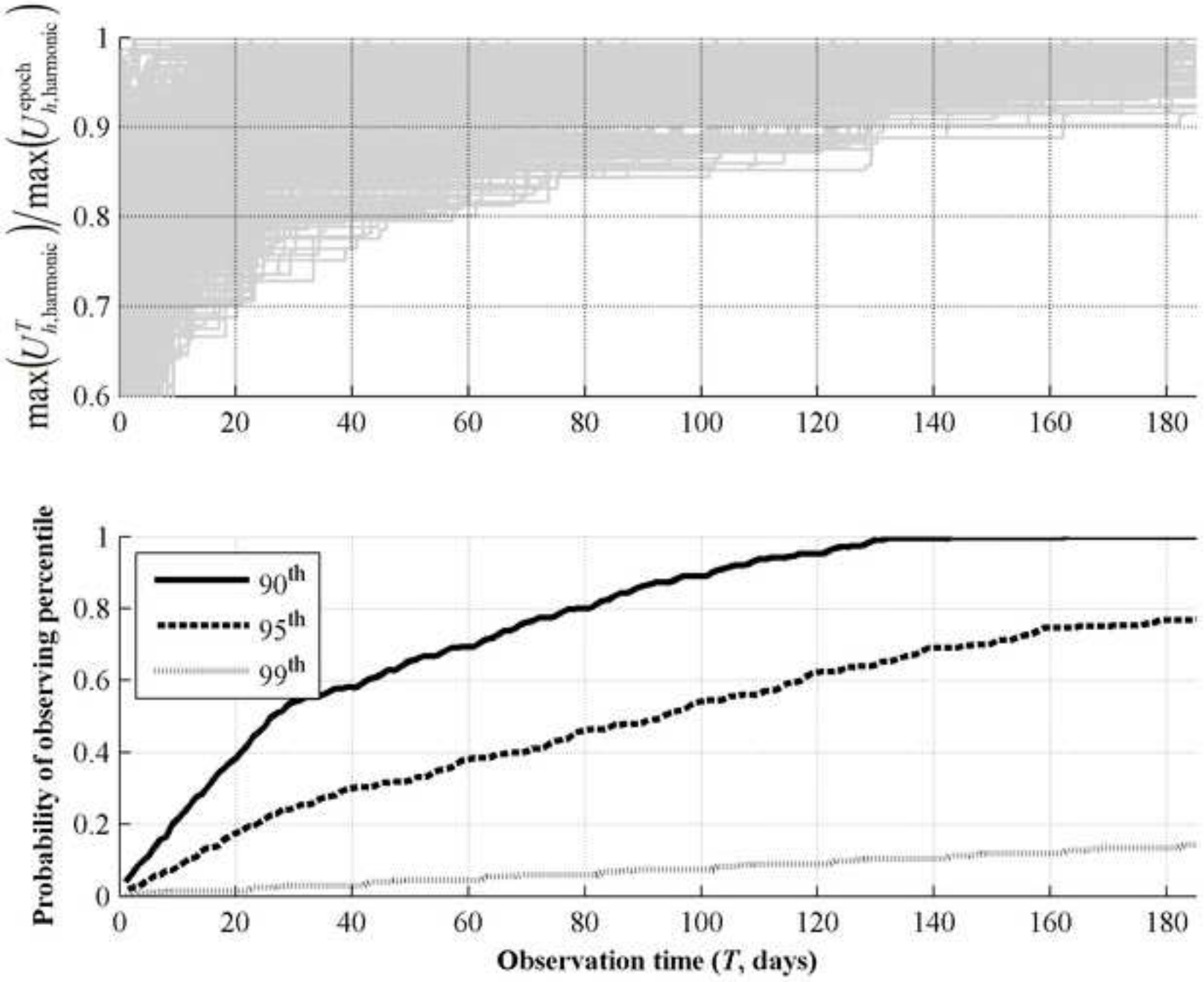

Figure5
Click here to download high resolution image

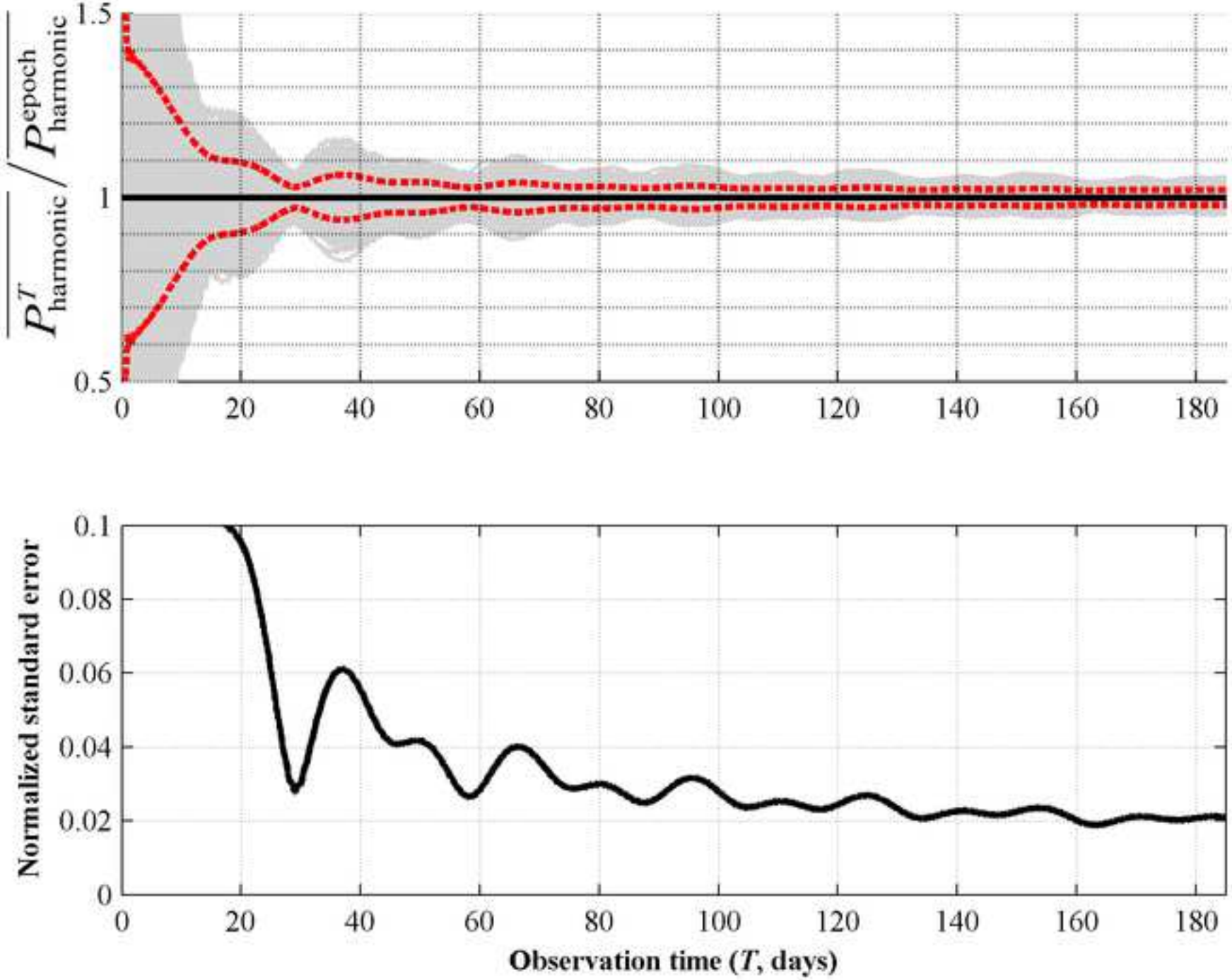

Figure6
Click here to download high resolution image

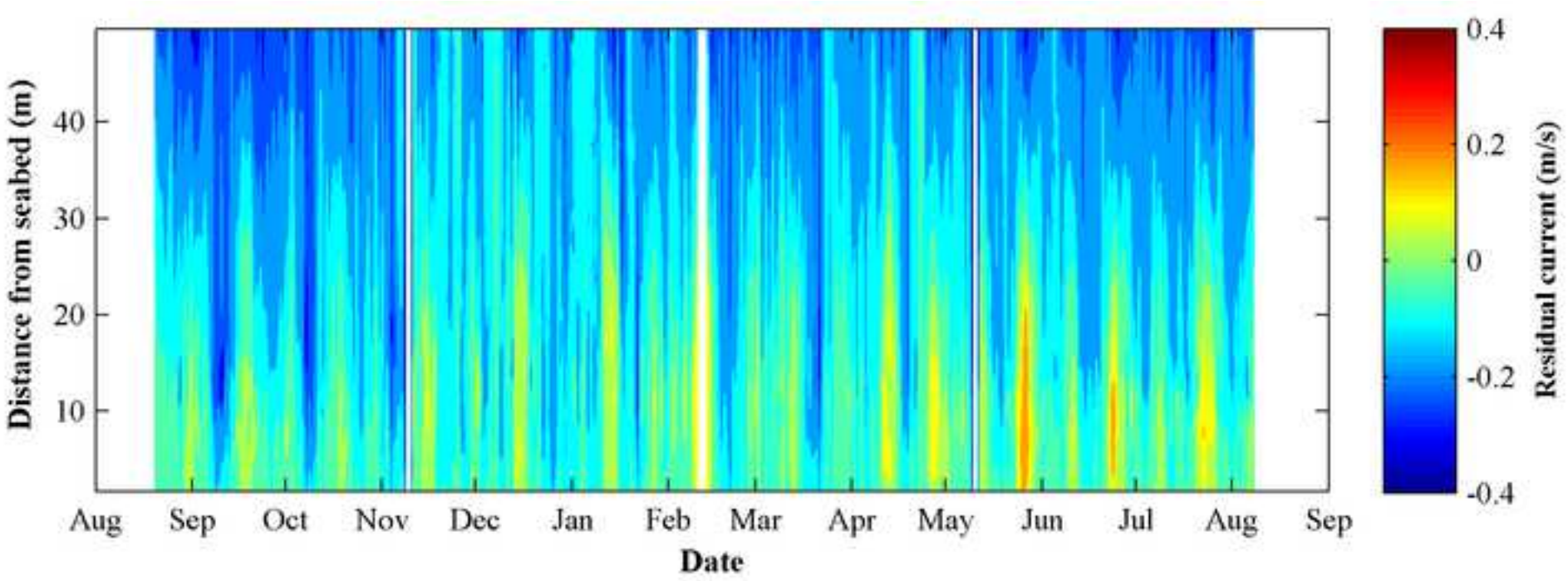

Figure7
Click here to download high resolution image

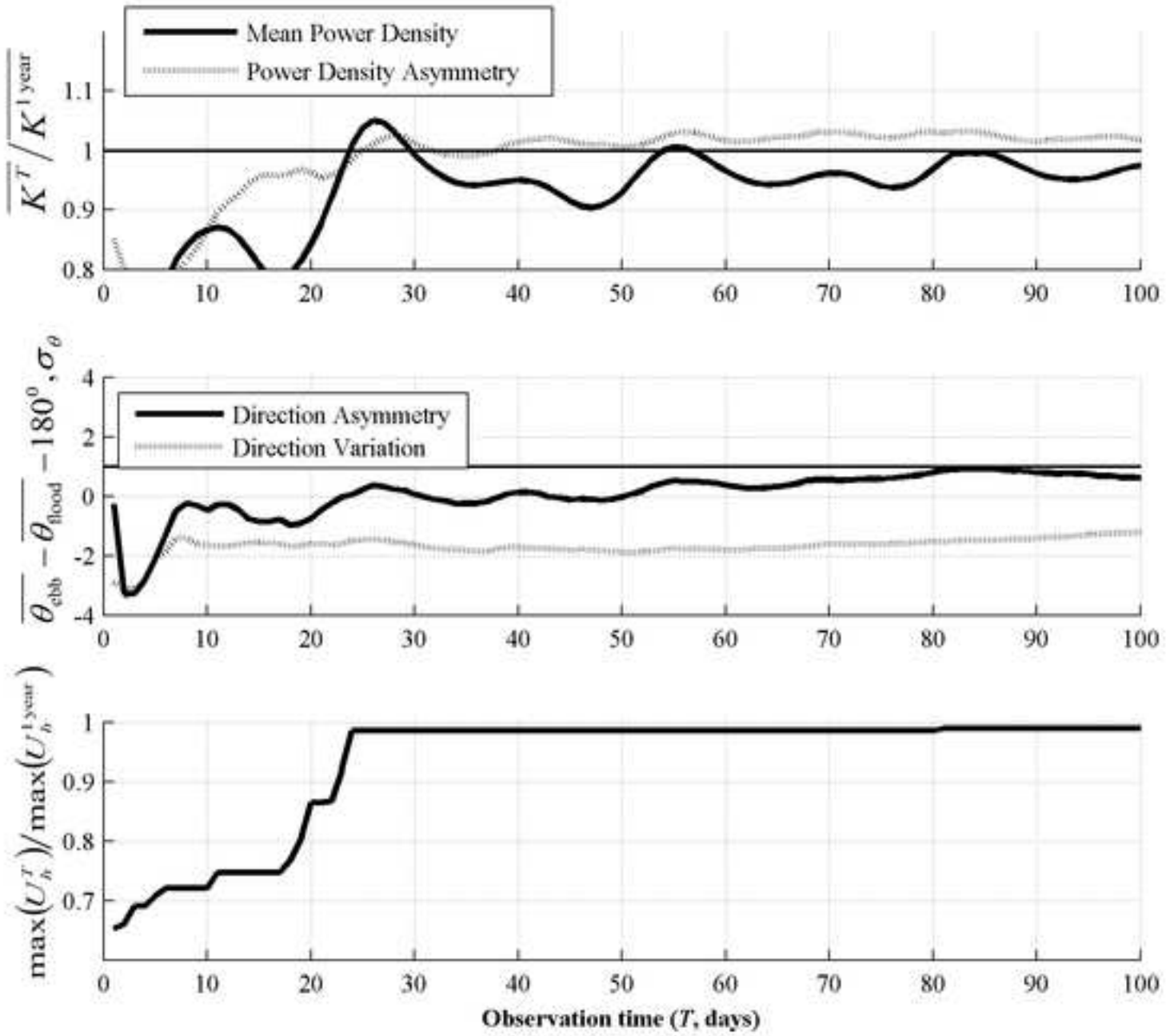

Figure8
Click here to download high resolution image

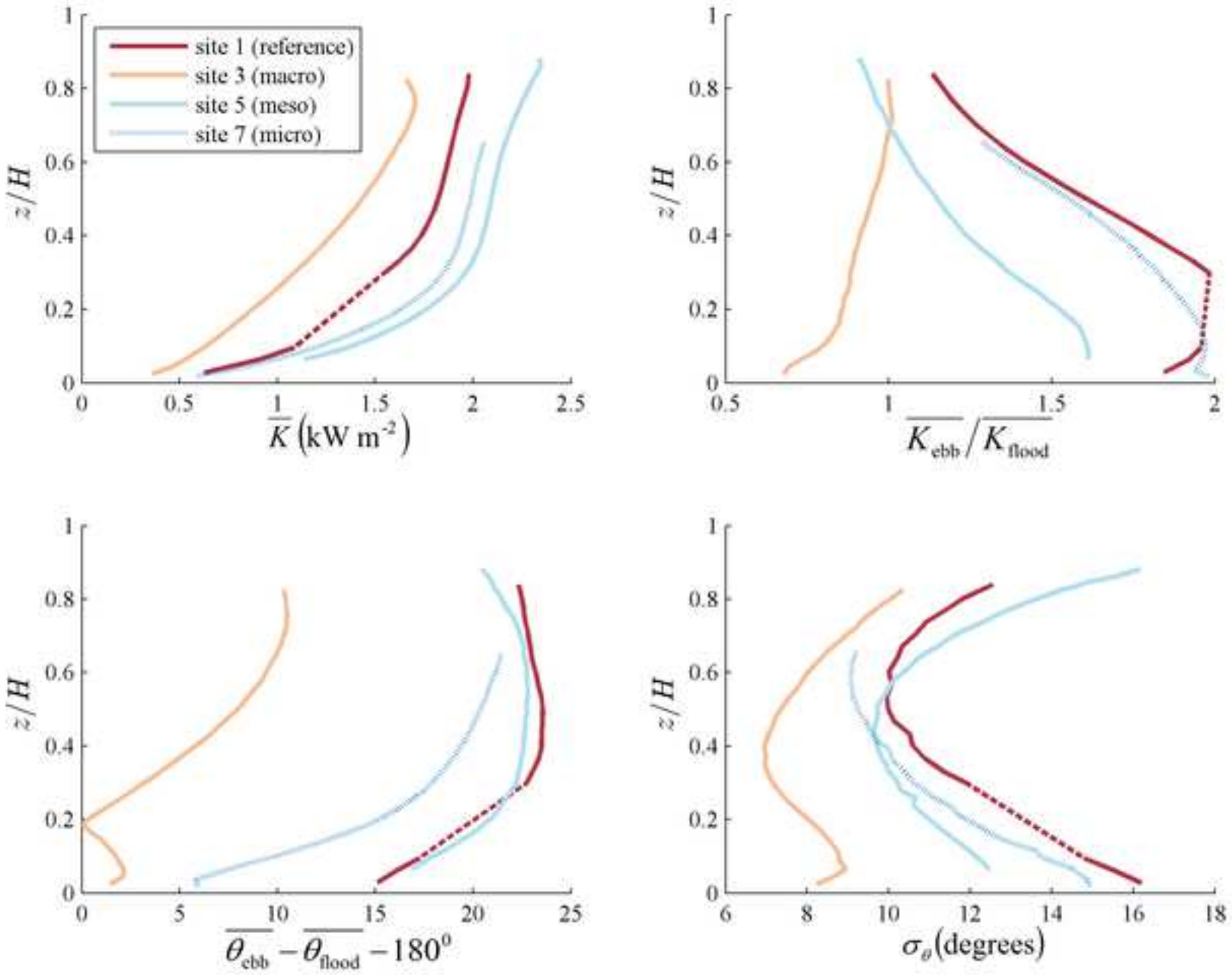

Figure9
Click here to download high resolution image

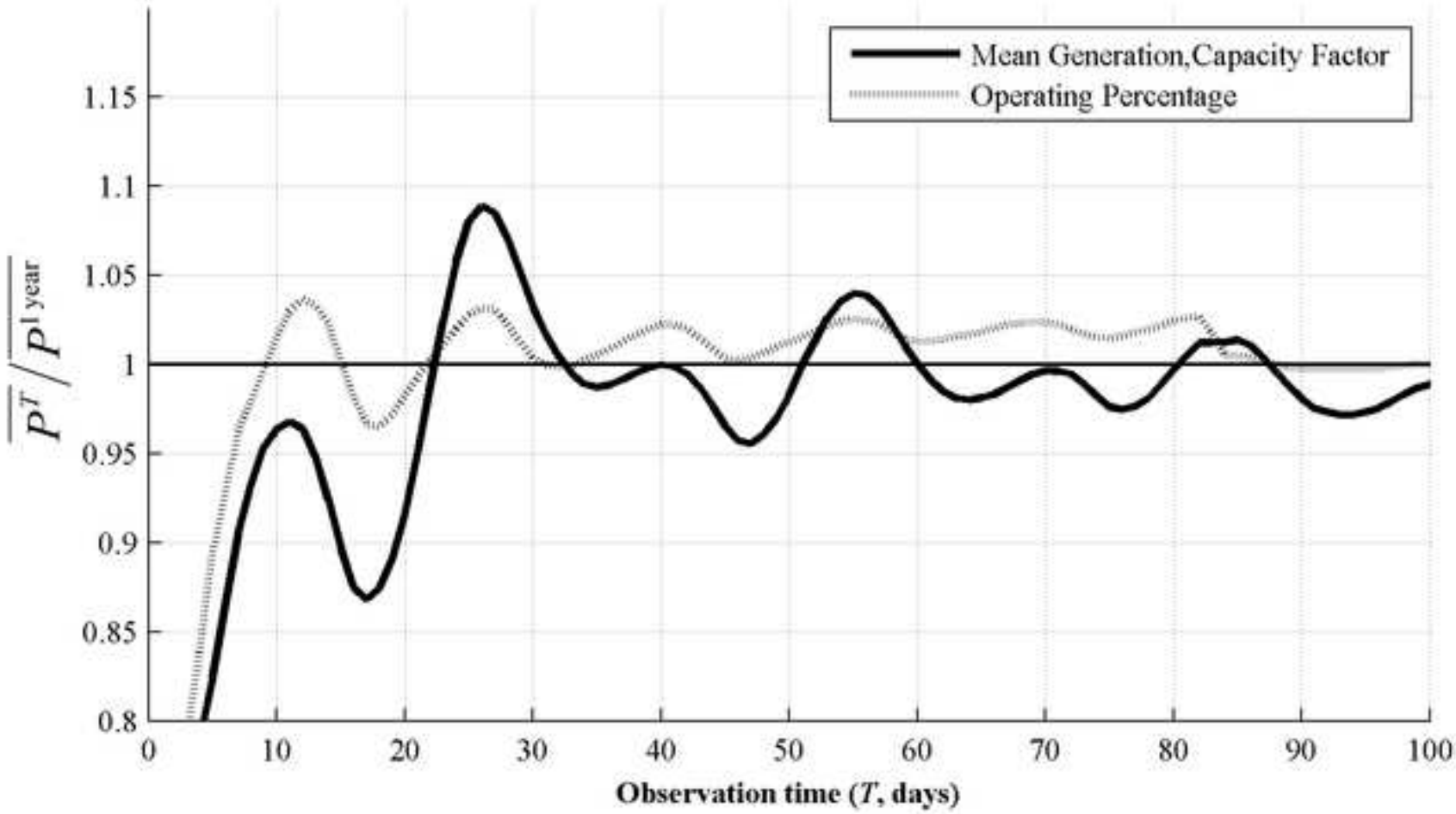

Figure10
Click here to download high resolution image

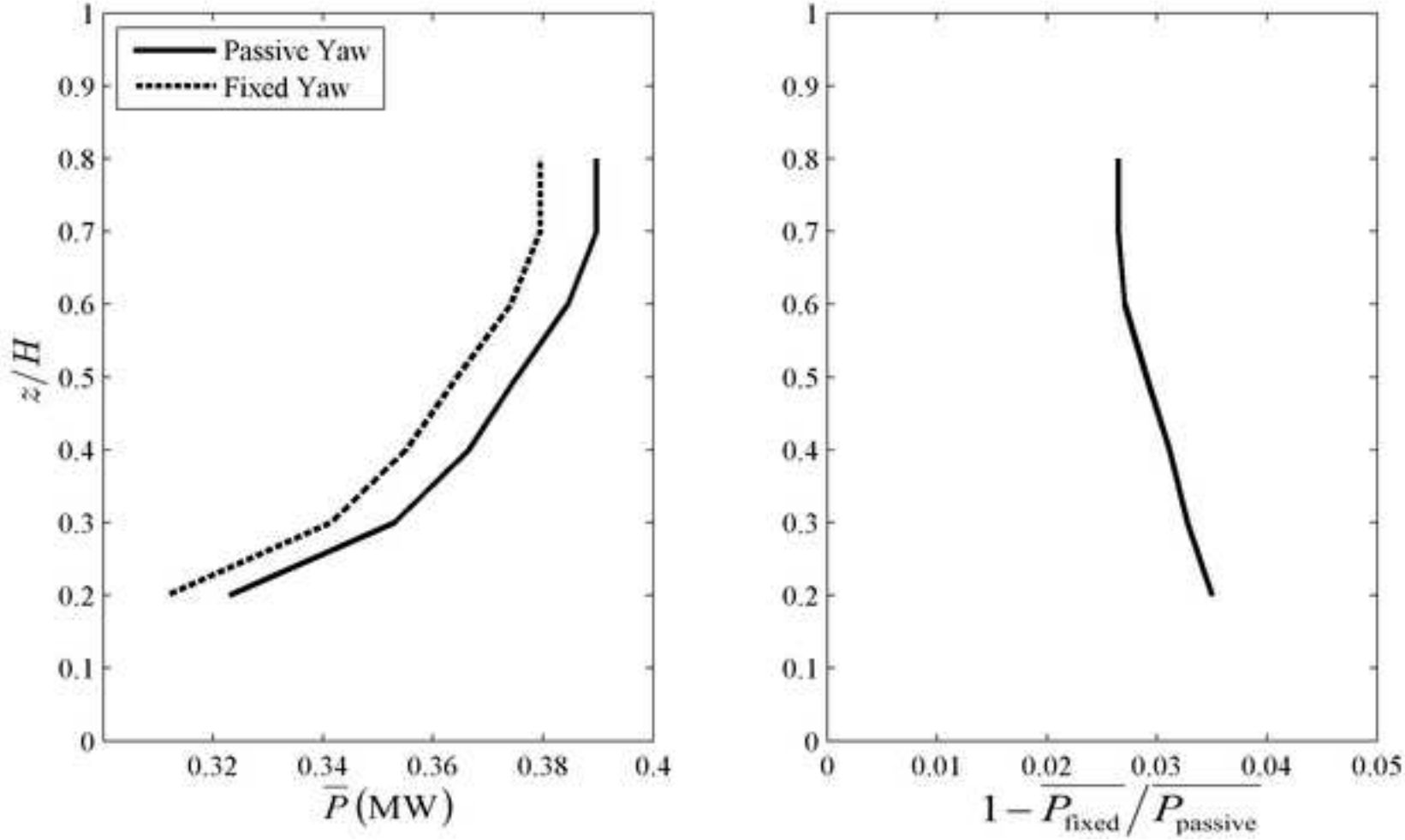

Figure11
Click here to download high resolution image